Journal of Power Sources 234 (2013) 302–309

Contents lists available at SciVerse ScienceDirect

Journal of Power Sources

journal homepage: www.elsevier.com/locate/jpowsour

A high-energy-density micro supercapacitor of asymmetric MnO_2–carbon configuration by using micro-fabrication technologies

Caiwei Shen [a,b], Xiaohong Wang [a,b,*], Siwei Li [a,b], Jian'gan Wang [a,c], Wenfeng Zhang [a,c], Feiyu Kang [a,c]

[a] Tsinghua National Laboratory for Information Science and Technology, PR China
[b] Institute of Microelectronics, Tsinghua University, Beijing 100084, PR China
[c] Department of Materials Science and Engineering, Tsinghua University, Beijing 100084, PR China

HIGHLIGHTS

- A micro supercapacitor of asymmetric MnO_2–carbon configuration is presented.
- Micro electrodes with different active materials are separated in a 3D structure.
- The device has an extended working voltage window and a large specific capacitance.
- It outperforms symmetric devices using either MnO_2 or activated carbon.

ARTICLE INFO

Article history:
Received 1 September 2012
Accepted 25 October 2012
Available online 9 February 2013

Keywords:
Micro supercapacitor
Energy storage device
Asymmetric electrodes
Manganese dioxide–activated carbon configuration

ABSTRACT

This paper demonstrates an asymmetric micro supercapacitor with superior overall performance that combines the advantages of both MnO_2 positive electrode and carbon negative electrode for energy storage on a chip. Nano-structured MnO_2 with rough surface is synthesized as active material for micro electrode. A self-supporting composite containing MnO_2 and another containing nanoporous activated carbon (AC) are separated in an interdigital structure by using micro-electro-mechanical systems (MEMS) fabrication technologies. Measurements of the prototype show that the asymmetric micro supercapacitor has well-performed capacitive behavior, and its working voltage range is extended from 1 V to 1.5 V in aqueous electrolyte due to the MnO_2–AC configuration. Calculations prove that it stores much higher energy densities than symmetric ones using either MnO_2 or AC. Moreover, this work provides an attractive approach to achieve various asymmetric micro energy storage systems on chips.

1. Introduction

The latest technology trends have shown growing interests in developing independent power supplies for wireless sensor networks, portable electronic devices and other self-powered micro systems, which particularly requires energy storage devices that can offer adequate energy and power with a lifetime matching that of the system being powered. Considering the demand of miniaturization and reducing the complexity of the whole system, designing energy storage elements that are miniaturized or even integrated with other parts is of great significance [1]. Although micro batteries have been studied as one of the solutions for those applications, they suffer from fundamental problems including relatively low charge/discharge rates and limited cycle lives (hundreds to thousands of cycles), which are caused by the volumetric electrochemical reactions they are based on [1,2].

Supercapacitor, as one of the energy storage devices used in diverse power systems, offers energy densities and power densities between those of batteries and conventional capacitors [3–5]. It finds applications when fast charge/discharge rates and long cycle lives (thousands to millions of cycles), as well as adequate energy densities are needed. Two kinds of supercapacitors are distinguished depending on the charge storage mechanisms. One is based on the electrical double layer (EDL) effect which stores static charges on the interface of high-surface-area electrodes and ion-containing electrolytes. Its electrode materials are represented by various nanoporous carbons. The other kind mainly relies on fast and reversible redox reactions that happen at the surface of active materials, and is known as pseudo capacitance. Transition metal oxides and electrically conducting polymers are examples of pseudo-capacitive electrode materials. The charge storage of EDL capacitors is fast but offers relatively low capacitance, while that of

* Corresponding author. Institute of Microelectronics, Tsinghua University, Beijing 100084, PR China. Tel.: +86 10 62798432; fax: +86 10 62771130.
E-mail address: wxh-ime@tsinghua.edu.cn (X. Wang).

0378-7753/$ – see front matter © 2013 Elsevier B.V. All rights reserved.
http://dx.doi.org/10.1016/j.jpowsour.2012.10.101

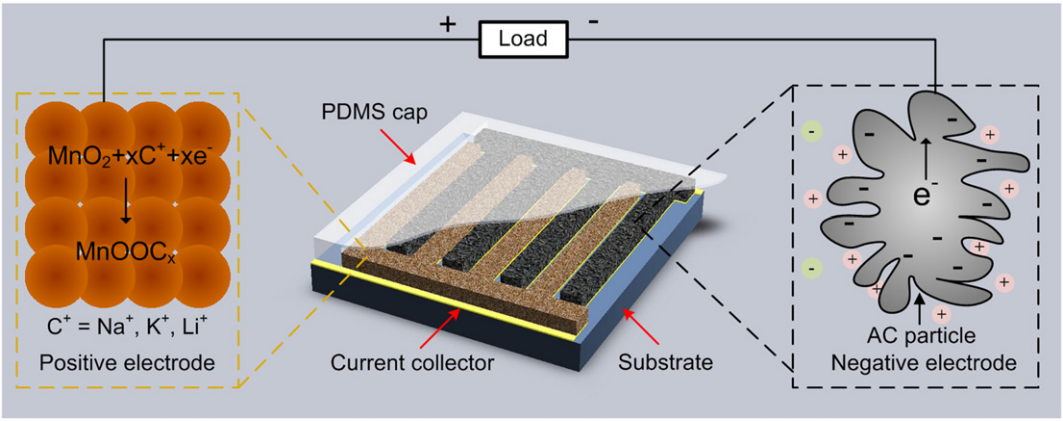

Fig. 1. Schematic of the asymmetric 3D micro supercapacitor using different active materials in interdigital electrodes. The charge storage and delivery mechanism of positive electrode (shown on the left) is based on reversible redox reactions of MnO_2, while that of negative electrode (shown on the right) is based on the EDL effect of highly porous activated carbon.

pseudo capacitors provides high capacitance but often delivers low power or suffers from poor cycle stability. The use and combination of both mechanisms are necessary to bridge the gap between batteries and conventional capacitors [3–7].

Studies in the past few years have demonstrated an attractive alternative to conventional EDL capacitors or pseudo capacitors by using hybrid systems that combines a high-energy electrode with a high-power electrode in the same cell [8,9]. The asymmetric design reaches outstanding performance because it offers high capacity via the Faradaic charge-storage mechanism of the positive electrode, and maintains fast charge/discharge rates due to the EDL capacitance mechanism at the negative electrode. Moreover, the asymmetric configuration can extend the operating voltage window of aqueous electrolytes beyond the thermodynamic limit (about 1.2 V), leading to significantly higher specific energy than symmetric ones using aqueous electrolytes. MnO_2–activated carbon (AC) supercapacitor is one of the representatives of those asymmetric systems, featuring high performance, low cost and environmentally friendly [10–13]. It was first proposed by Hong et al. [10], and then intensively studied and improved afterward [11–14]. The MnO_2–AC device has achieved high energy and power densities (10 Wh kg^{-1} and 16 kW kg^{-1}) over long cycles (nearly 200,000 cycles) for practical application [13], and an interesting fact is that the capacity of the present MnO_2 material is still far from being fully exploited comparing to its theoretical value [4,15,16].

Micro-supercapacitors are also developed in recent years, expected to couple with micro batteries and energy harvesting systems on chips to deliver or harvest the peak power, or replace batteries for micro energy storage [17–25]. They have not just been scaled down from large-sized ones, and good micrometer-sized electrode structures are especially important to improve their performance. Because footprint areas are limited for micro systems on those occasions, three-dimensional (3D) electrodes that are scalable on the surface of substrate and extensible from the third dimension become basic solutions [1,2]. Micro supercapacitors with 3D electrodes have been developed in many cases, and both EDL capacitors [17–23] and pseudo capacitors [24,25] have been studied. However, they are all based on symmetric design that uses identical materials as both positive and negative electrodes, and either EDL or pseudo capacitance is mainly involved. Although a variety of supercapacitors with asymmetric electrodes can provide excellent overall performance [8,9], they are rarely reported as solutions for micro energy storage, probably because that their micro fabrication, i.e. building 3D electrodes with micro-meter separation, is a great challenge.

Here we report an asymmetric micro supercapacitor using MnO_2–AC configuration with 3D interdigital electrode structure, and it is an on-chip device based on MEMS fabrication technologies. Such design is expected to take advantages of both the

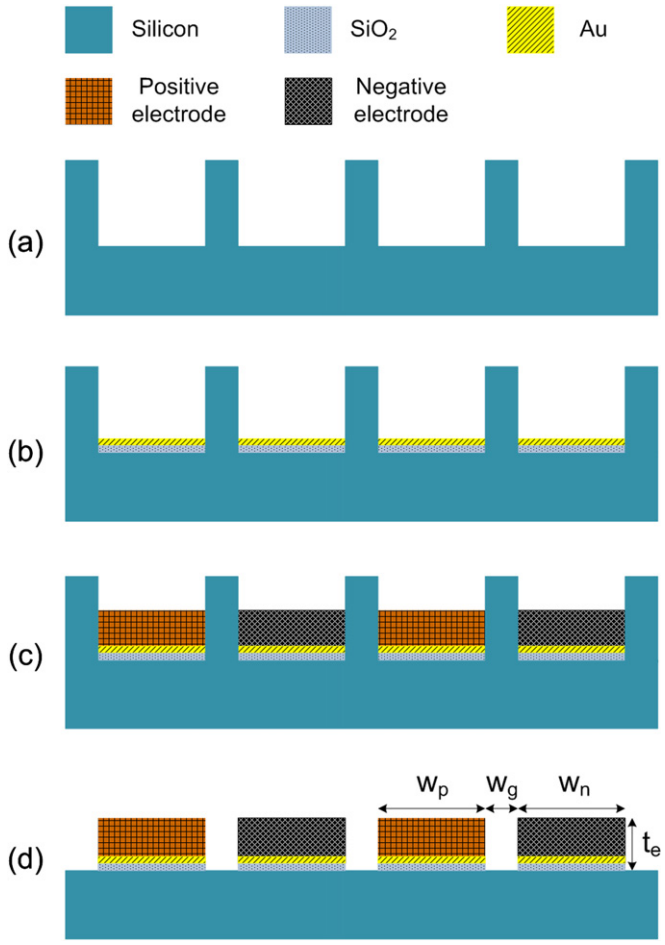

Fig. 2. Cross-section illustration of fabrication process of the asymmetric micro supercapacitor. (a) Etching of interdigital channels on silicon substrate; (b) deposition of a layer of SiO_2 and a layer of Au, and the unwanted layers on top of the silicon wall are partially etched; (c) filling of positive and negative electrode materials into the separated channels; (d) etching of the wall between electrodes. The resulting widths of positive electrode, negative electrode, and the gap between electrodes, are w_p, w_n, and w_g, respectively, and the thickness of electrodes is t_e.

high-capacitance MnO_2 and high-power AC so that overall performance superior to that of symmetric micro supercapacitors can be achieved.

2. Design and materials

2.1. Structure design

It has been demonstrated that the micrometer-sized electrode structure is of considerable importance to micro supercapacitors [22]. Enough material should be loaded on a limited surface to store adequate energy and the positive and negative electrodes should be close to keep ion-transport path short. Taking the scalability and extensibility of the structure into consideration, the device was designed as illustrated in Fig. 1, in which positive and negative electrodes are separated in a 3D interdigital structure. Particles of MnO_2 in the positive electrode use a reversible redox reaction to serve as the energy source, and porous activated carbon in the negative electrode stores charges in EDL and is able to offer fast power.

The structure can be achieved by applying fabrication process illustrated in Fig. 2, which is based on strategies proposed in our previous work [22]. Interdigital channels separated by a wall are first etched on the substrate, and then self-supporting electrode materials are filled into channels after deposition of an insulation layer and a current collection layer. The wall is finally etched to create a gap between electrodes. The device is scalable on the substrate plane, where widths of positive electrode, w_p, and negative electrode, w_n, as well as the gap between electrodes, w_g, are adjusted by patterns of photomasks used in lithography. The thickness of electrodes, t_e, is also adjustable depending on the depth of etched channels as well as the amount of materials filled into the channels. The performance of the device can be better by designing smaller w_g, but it is limited by the precision of fabrication technology. To demonstrate the basic idea of building asymmetric micro supercapacitor, as well as to ensure the stability of the fabrication process, the practical device of Fig. 1 was designed to be constructed with 20 interdigital fingers (10 fingers per polarity), and each finger was 90 μm wide and 10 μm thick with a 30 μm-wide gap between them, which means $w_p = w_n = 90$ μm, $w_g = 30$ μm, and $t_e = 10$ μm.

2.2. Electrode materials

As MnO_2 stores energy using fast redox reactions that happen on or near the surface of the material, nano-structured MnO_2 can offer higher capacity by providing larger specific surface area. Various forms of nano-structured MnO_2 have been reported [26], including crystals and composites. Some of them have large gravimetric capacitances and some even close to the theoretical specific capacitance of MnO_2 (about 1300 F g^{-1}) [4,15], but they suffer from either low volumetric capacitances, which is essentially unsuitable for micro-scale applications, or not being compatible with micro fabrication. In fact, the reported MnO_2 materials with extremely large capacitances are mostly very thin layers with thicknesses of a few nanometers, and their performances deteriorate seriously when used to construct thicker electrodes, making them unsuitable for building micrometer-sized 3D electrodes.

We used a facile way to prepare the positive electrode material with desired properties. Pure nano powder of MnO_2 was synthesized by reacting $KMnO_4$ with Polyethylene Glycol (PEG 400) in water. In a typical procedure, 4.00 g $KMnO_4$ was first dissolved in 400 mL deionized water and then PEG was dropped to the solution while stirring. Several more drops were added after the fuchsia color of the solution faded to ensure a fully transformation from $KMnO_4$ to MnO_2. Then the precipitate was filtered, washed with both ethanol and deionized water for several times and finally dried at 60 °C. In the reaction, $KMnO_4$ was reduced and produced

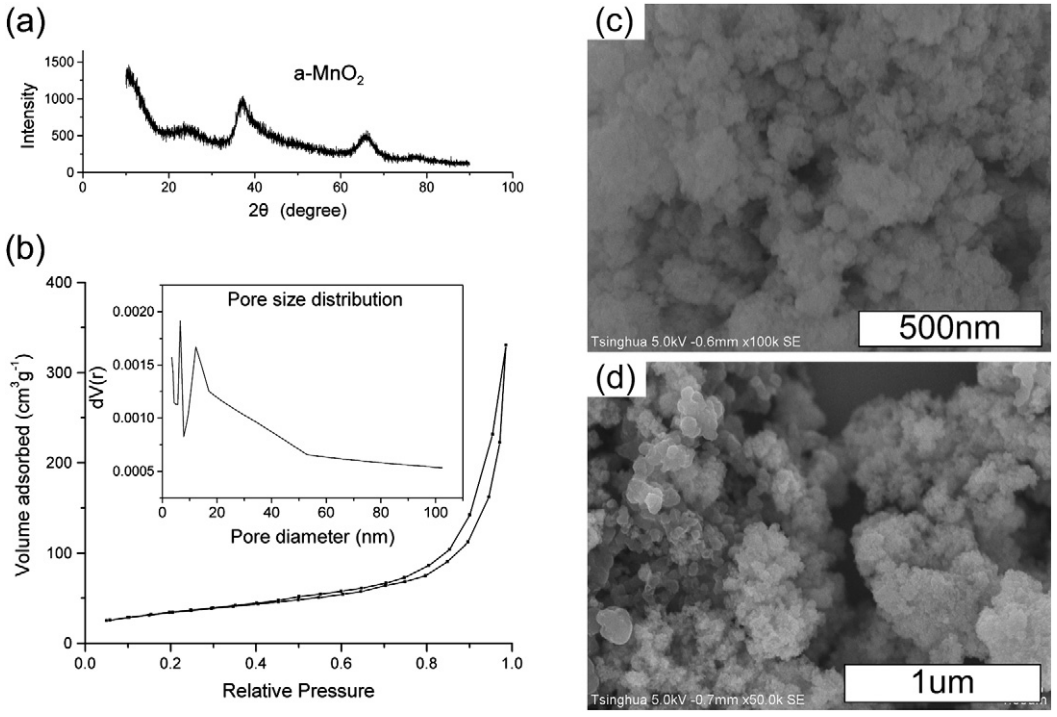

Fig. 3. (a) XRD pattern of the synthesized MnO_2; (b) the nitrogen adsorption–desorption isotherm of the MnO_2, with inset showing corresponding pore size distribution which was calculated based on the BJH method using the adsorption isotherm; (c) SEM image of the pure nano-structured MnO_2, in which the particles are densely packed and have rough surfaces; (d) SEM image of the composite electrode material containing MnO_2, carbon black and PVDF in a weight proportion of 8:1:1.

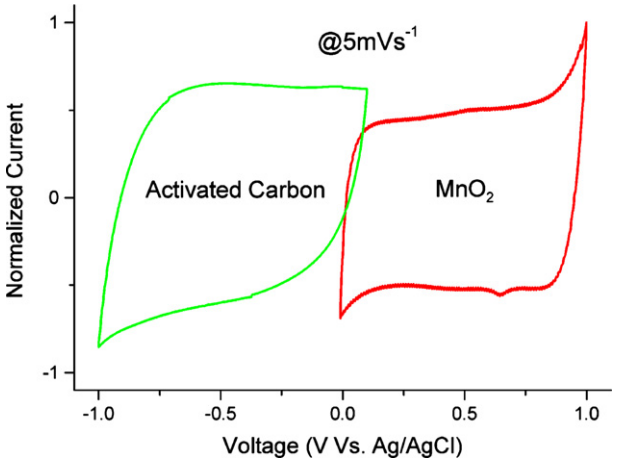

Fig. 4. Cyclic voltammetry (CV) curves of the composite containing MnO_2 working in the positive voltage range and the composite containing activated carbon working in the negative voltage range. The curves were measured in a three-electrode system and currents are normalized.

MnO_2 precipitate, and PEG served as not only reductant but also dispersant. Particles of MnO_2 were protected by it from aggregating, resulting in nano-sized spheres.

Fig. 3(a) shows the X-ray diffraction pattern of the as-synthesized precipitate, indicating an amorphous phase that is similar to other manganese oxides synthesized by precipitation reactions in water [27]. The porosity of the material is characterized by analysis of nitrogen physisorption test. The nitrogen adsorption–desorption isotherm of the MnO_2 is presented in Fig. 3(b), with inset showing corresponding pore size distribution. The pore size distribution was calculated based on the Barrett–Joyner–Halenda (BJH) method using the adsorption isotherm. It can be seen that the MnO_2 is mainly mesoporous and its pores are mostly of diameters less than 40 nm. The Brunauer–Emmett–Teller (BET) surface area of the material is 130 $m^2\ g^{-1}$, also calculated from the adsorption–desorption isotherm. The MnO_2 was observed by scanning electron microscopy (SEM), and the corresponding image is shown in Fig. 3(c). The MnO_2 particles with diameters of tens of nanometers are densely packed and have rough surfaces that can further expand the surface area. This image also explains the profile of the pore size distribution curve in Fig. 3(b), in which the broad peak at more than 10 nm is caused by pores between nano particles, while the peak at less than 10 nm is due to rough surface of the particles.

In order to build a 3D micro structure, the electrode material is expected to be self-supporting. One approach to form self-supporting electrode is using composite that contains the active material and a binder [22]. In this work, the MnO_2 was mixed with carbon black (as a conductive agent) and PVDF (as a polymer binder) in a weight proportion of 8:1:1. The mixture was then dispersed in *N*-methyl-2-pyrrolidone (NMP) and finally became a self-supporting electrode material by evaporating the solvent. The SEM image of the composite is shown in Fig. 3(d). The capacitance property of the composite was measured in a three-electrode configuration, where the working electrode is a gold foil with the dried composite (about 10 μm thick) adhered to it, the counter electrode is a Pt foil, the reference electrode is Ag/AgCl electrode, and 0.2 M K_2SO_4 solution was used as electrolyte. From the cyclic voltammetry curve at a scanning rate of 5 mV s^{-1}, a specific capacitance of 160 F g^{-1} for the composite and about 200 F g^{-1} for the pure MnO_2 can be calculated. We also measured capacitances of the composite with different thicknesses. The composite is pressed onto several nickel foils to form working electrodes, and thicknesses of the electrodes range from 50 μm to 150 μm. The electrodes are all tested in the three-electrode system described above, and show capacitances around 150–160 F g^{-1}, independent of the thickness.

It has been proved that MnO_2 is not an optimal material for both positive and negative electrodes in symmetric capacitors, but it exhibits high performance in an asymmetric configuration with AC as negative electrode [10–14]. A nanoporous AC (1000 $m^2\ g^{-1}$, BET) was therefore used in this work, and a composite containing AC, carbon graphite and PVDF in a weight proportion of 8:1:1 was applied as the electrode material. The electrochemical property of the composite was also tested in a three-electrode system using 0.2 M K_2SO_4 solution as electrolyte. The working electrode was the composite pressed onto a nickel foil with a thickness of about 150 μm and the measured capacitance is 100 F g^{-1}. Cyclic voltammetry curves of two composites containing either MnO_2 or AC as active material are presented in Fig. 4, each showing capacitive behavior in different working voltage ranges.

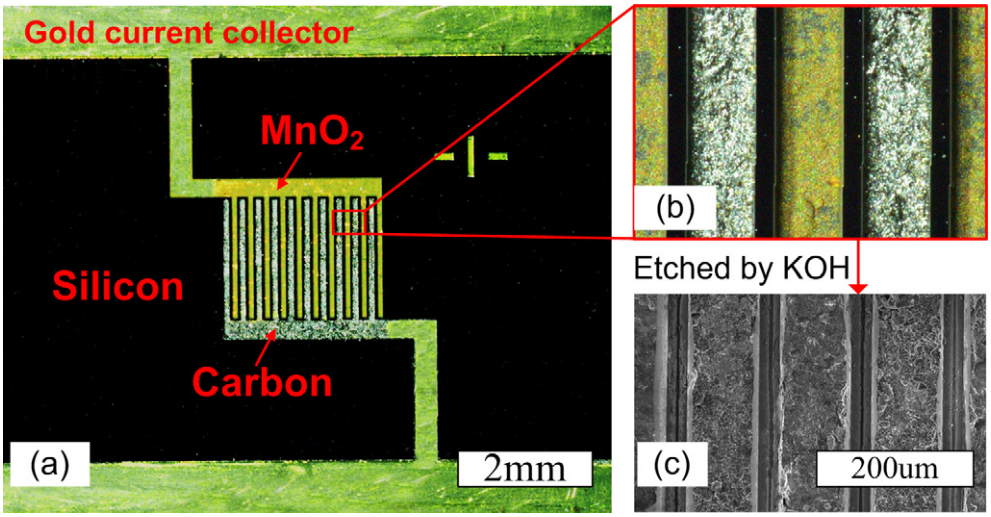

Fig. 5. (a) Photo of a prototype with two electrode materials filled into the interdigital channels; (b) a magnified photo showing electrodes with different materials separated by a silicon wall; (c) SEM image of the electrodes when the silicon wall has been etched by KOH.

Table 1
Summary of parameters of the fabricated micro supercapacitor.

Sizes of the interdigital electrodes	w_p	90 μm
	w_n	90 μm
	w_g	30 μm
	t_e	10 μm
	l_e	1800 μm
Total effective area		2.4 mm × 2.4 mm

w_p, w_n, w_g, t_e are parameters illustrated in Fig. 2(d). l_e is the length of each interdigital finger.

3. Fabrication

The detailed fabrication process of the micro supercapacitor, which follows the basic steps illustrated in Fig. 2, is described as below. Silicon substrate was etched by inductively-coupled plasma to form 3D interdigital channels. The designed channels were 50 μm deep, and fingers of the interdigital channels were 90 μm wide, 1800 μm long and separated by a 30 μm-wide silicon wall. A 300 nm thick SiO_2 as insulation layer and then a 100 nm thick gold layer were deposited and partially etched, so that the gold served as current collector at the bottom. A composite containing MnO_2 and another containing AC, both were dispersed in NMP, were injected into the separated channels respectively, and then dried under 80 °C to become self-supporting electrodes. As the material shrank after the solvent evaporated, the actual thickness of electrodes was about 10 μm. Of course, thicker electrodes can be achieved by fabricating deeper channels as well as repeating the injecting-drying process for more times [22]. We did the injecting-drying process for only one time simply to ensure the stability of the fabrication process. The photo of a cell with different electrode materials in the interdigital channels is shown in Fig. 5(a) and (b), fingers of the electrodes are separated by a silicon wall. The silicon wall was finally etched by KOH solution and the space was left for the electrolyte. SEM image of the fabricated electrodes is shown in Fig. 5(c). The prototype was then sealed by a PDMS cap, with electrolyte (0.2 M K_2SO_4) injected into the effective area (2.4 mm × 2.4 mm interdigital area in the middle of the cell). Sizes of the fabricated micro supercapacitor are summarized in Table 1.

Two symmetric supercapacitors of the same sizes using either MnO_2 or AC were also fabricated to compare with the asymmetric one. The fabrication processes were the same, except that one used MnO_2 as both positive and negative electrodes, the other used AC.

4. Results and discussion

4.1. Electrochemical property of the asymmetric micro supercapacitor

Electrochemical properties of all the prototypes were characterized by PARSTAT 2273 (AMETEK, Inc.) electrochemical analysis system. One obvious advantage of asymmetric supercapacitor deduced from cyclic voltammetry (CV) curves is the extension of operating voltage window. Fig. 6 shows the CV curves of the asymmetric prototype under different voltage scanning rates from 20 mV s^{-1} to 200 mV s^{-1}. As CV curves of ideal capacitors are rectangular [3], the well-performed capacitive behavior of this device is indicated by the nearly parallelogram shape, and the shape is almost preserved when working voltage range is extended from 1 V to 1.5 V at every scanning rate. But in symmetric supercapacitors with aqueous electrolytes, the operating voltage window is usually no more than 1 V (the thermodynamic window of water is 1.23 V).

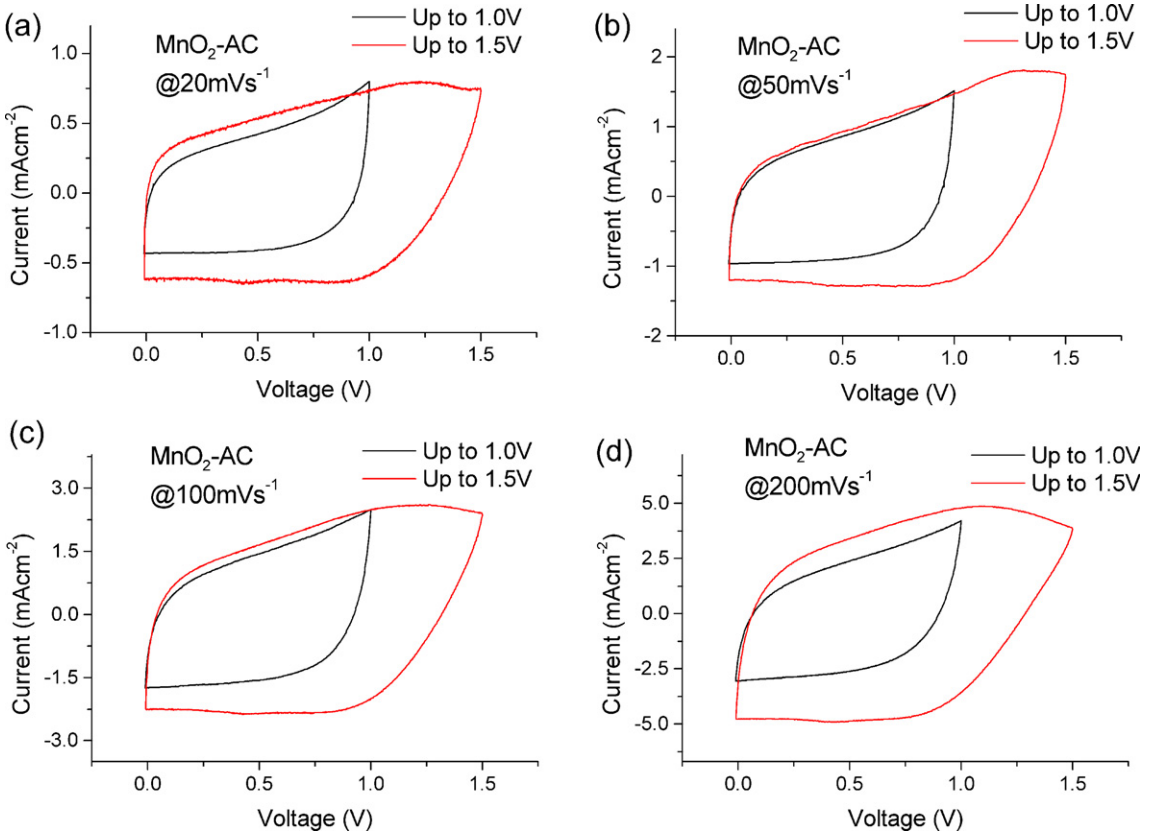

Fig. 6. CV curves of the asymmetric supercapacitor with voltage scanning ranges of 1 V and 1.5 V, the scanning rate is (a) 20 mV s^{-1}; (b) 50 mV s^{-1}; (c) 100 mV s^{-1}; (d) 200 mV s^{-1}. The nearly parallelogram shape is preserved at each scanning rate with different voltage scanning ranges.

4.2. Capacitances of three prototypes

The electrochemical behaviors of two symmetric supercapacitors are also tested, and their CV curves working at various scanning rates in 1 V are shown in Fig. 7(a) and (b). It is obvious that CV curves of the MnO_2–MnO_2 supercapacitor in Fig. 7(a) are close to rectangle at a low scanning rate of 20 mV s^{-1} but deform seriously when scanning rates are higher. On the other hand, the shape of curves of the AC–AC device in Fig. 7(b) does not deform much when scanning rate changes. This phenomenon proves that the property of MnO_2 is a major restriction of power performance of a device. The low conductivity of MnO_2 and the Faradaic reaction limit the charge/discharge rate of the MnO_2 electrode, and make it slower than non-Faradaic charge storage in highly conductive AC.

The higher operating voltage makes the asymmetric supercapacitor store more energy than symmetric ones, but its rate capacity is still between the two. This can be qualitatively observed in Fig. 7(c), in which CV curves of three supercapacitors under a high scanning rate of 200 mV s^{-1} are presented. The CV curve of symmetric MnO_2–MnO_2 supercapacitor has deviated from parallelogram, but that of AC–AC one still resembles rectangle, and that of asymmetric supercapacitor is between the two.

Specific capacitances (C) can be calculated from CV curves according to Formula (1):

$$C = \frac{\int I\mathrm{d}t}{\Delta V} = \frac{\int I\mathrm{d}V}{\Delta V \times r} \tag{1}$$

where I is the measured current on the CV curves, ΔV is the voltage range and $r = \mathrm{d}V/\mathrm{d}t$ is the voltage scanning rate. The calculated capacitances of three devices depending on scanning rates are plotted in Fig. 7(d). For the asymmetric device, capacitances under different working voltage ranges are also compared. The quantitative analysis verifies that the MnO_2 material limits the power performance of devices. The capacity of MnO_2–MnO_2 supercapacitor drops from 28.3 mF cm^{-2} to 5.6 mF cm^{-2}, which retains only 19.9% of capacitance, when scanning rate rises from 20 mV s^{-1} to 500 mV s^{-1}. And that of AC–AC drops from 15.6 mF cm^{-2} to 8.8 mF cm^{-2}, with a retention of 56%. The capacity of the MnO_2–AC supercapacitor, however, shows the intermediate value and tendency when the device works in 1.0 V, which drops from 21.3 mF cm^{-2} to 7.8 mF cm^{-2}, with a retention of 36%. Accordingly, it can be inferred that using high-capacity MnO_2 as positive electrode and high-power AC as negative electrode can produce the balanced performance of the device, in terms of both capacity and power, when working at the same condition. The change of working condition, which is the working voltage range in this case, can make the calculation results different. The asymmetric supercapacitor has larger calculated capacitance when working in a voltage range of 1.5 V, the value is from 30.0 mF cm^{-2} to 12.8 mF cm^{-2}, retaining 43% at the highest scanning rate. As Formula (1) estimates the average capacitance within the working voltage range, the asymmetric device working in 1.5 V can store more charge in average than working in 1.0 V, and can store even more energy (E) than estimation that is based on the traditional formula for capacitors:

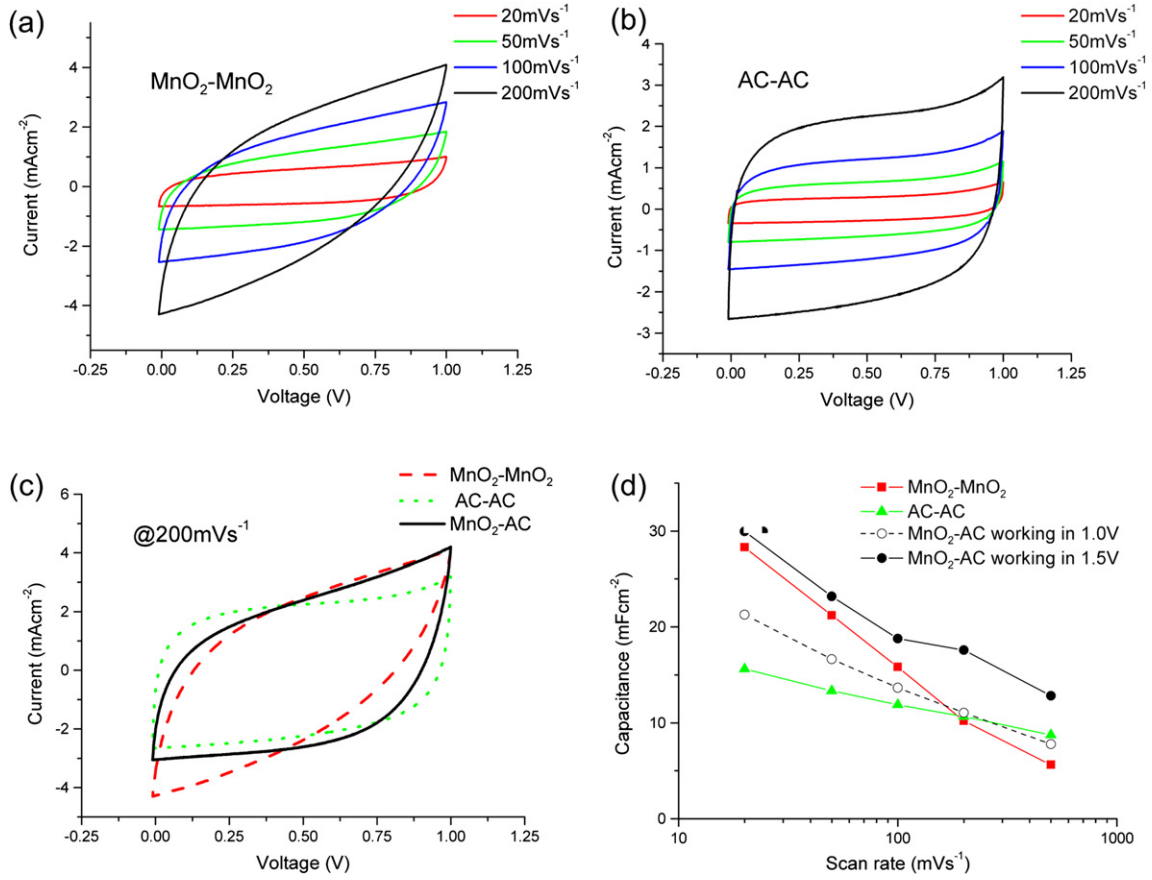

Fig. 7. CV curves of the (a) MnO_2–MnO_2 and (b) AC–AC symmetric device under scanning rates ranging from 20 mV s^{-1} to 200 mV s^{-1}; (c) comparison of CV curves of three prototypes under a high scanning rate of 200 mV s^{-1}, and the voltage range is from 0 to 1 V; (d) calculated capacitances under various scanning rates showing distinct variation tendencies for three prototypes, while for the asymmetric device, the capacitance value and variation tendency are different when the voltage scanning range changes from 1.0 V to 1.5 V.

$$E = \tfrac{1}{2}CV^2 \quad (2)$$

where the capacitance C is usually unchanged and the energy is proportional to voltage squared.

Note that the capacitance per unit area is proportional to the amount of electrode material loaded on the substrate. As a result, the capacitance of the device can be directly enlarged by building thicker electrodes with narrower gap in between so that more electrode material can be loaded per area. This can be verified by comparing the capacitance of AC–AC supercapacitor (15.6 mF cm^{-2}, with 10 μm-thick electrodes and a 30 μm-wide gap) to the result in our previous work [22], in which the device shows a capacitance of 90.7 mF cm^{-2} (with 50 μm-thick electrodes and a 15 μm-wide gap) using the same electrode material.

4.3. Comparison of the overall performances

To evaluate the overall performances of three micro supercapacitors, quantitative calculations of the energy (E) and power (P) of three prototypes are made based on their CV tests under various scanning rates, according to the following equations:

$$E = \int VI\mathrm{d}t = \frac{1}{r}\int VI\mathrm{d}V, \quad (3)$$

$$P = \frac{E}{\Delta t} = \frac{E \times r}{\Delta V}, \quad (4)$$

where V is the voltage, I is the measured current, t represents the time and r is the voltage scanning rate. Because of their different operating voltage windows, V is from 0 to 1.5 V for asymmetric supercapacitor, and 0–1 V for symmetric ones. As volumetric energy and power densities are of more significance in this work, they are derived by considering the effective volume of the electrodes. We take only the 2.4 mm × 2.4 mm effective area of the prototypes including areas of the electrodes and the gap, and the electrode thickness of 10 μm into consideration, while the volumes of substrate, package and other parts are not included. The calculated results based on CV curves with scanning rates from 20 mV s^{-1} to 500 mV s^{-1} are plotted in Fig. 8, which is also known as Ragone plots. It can be deduced from the plots that the AC–AC capacitor exhibits the best rate capacity, but its energy density is relatively low because of the smaller specific capacitance of AC.

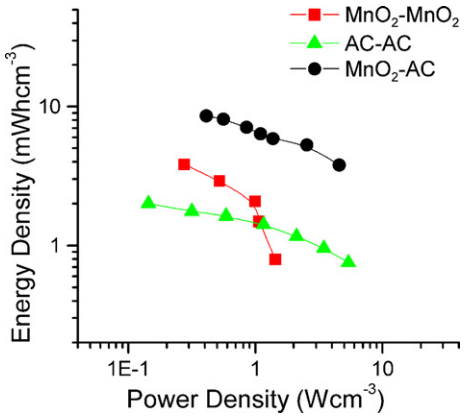

Fig. 8. Ragone plots of three prototypes, in which each point of a prototype is calculated from a CV curve of that prototype under a certain scanning rate. The range of scanning rates is from 20 mV s^{-1} to 500 mV s^{-1}. The voltage range of prototypes with symmetric electrodes is from 0 to 1 V, and that of asymmetric prototype is from 0 to 1.5 V.

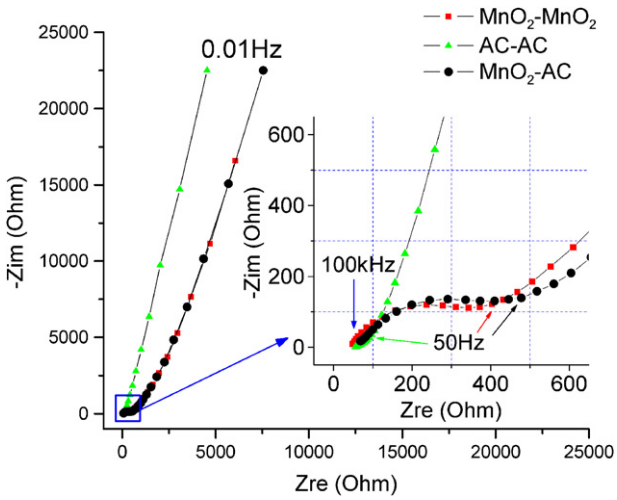

Fig. 9. Nyquist plots of three prototypes with a high-frequency inset, measured at a bias of 0 V, under frequencies from 0.01 Hz to 100 kHz.

The MnO_2–MnO_2 supercapacitor stores more energy when working at low power, and its performance drops quickly as the power increases, further proving the limited conductivity of MnO_2. The asymmetric supercapacitor shows the highest energy density (about 4 times higher than that of AC–AC capacitor) because of its extended operating voltage as well as the large specific capacitance illustrated in Fig. 7(d). Its rate capacity, almost as good as the AC–AC capacitor, is much better than the MnO_2–MnO_2 device, indicating a balanced result.

4.4. Electrochemical impedance spectra measurements

Electrochemical impedance spectra of three prototypes were measured, and Fig. 9 shows the corresponding Nyquist plots. The imaginary parts of all curves increase quickly from 50 Hz down to 0.01 Hz, indicating a capacitive behavior of all devices. The AC–AC capacitor has the lowest resistance due to the highly conductive nature of the carbon material. The other two capacitors have very similar impedances. As two electrodes of a device are in series, impedance of MnO_2–AC device is the combination of the MnO_2 electrode and the AC electrode, and it can be deduced that its high resistance is mainly caused by the MnO_2 electrode.

5. Conclusions

A high-energy-density asymmetric micro supercapacitor using MnO_2 and AC as positive and negative electrode, respectively, is demonstrated. Nano-structured MnO_2 with desired properties was synthesized in a facile way. The self-supporting composite containing as-synthesized MnO_2 was separated with another composite containing nanoporous AC in an interdigital structure by using MEMS technologies. Compared to two symmetric supercapacitors using either MnO_2 or AC, the asymmetric supercapacitor has superior overall performance and especially stores higher energy densities because of possessing both a larger capacitance and an extended operating voltage range. As studies have shown that this kind of asymmetric configuration can be optimized by carefully adjusting the mass ratio of positive and negative electrode materials [14], the results in this paper can be further improved. Moreover, this work provides an attractive approach to achieve various asymmetric micro energy storage systems on chips.

Acknowledgments

This work is supported by the National Natural Science Foundation (No. 60936003), 973 program (No. 2009CB320304), and 863 program (No. 2009AA04Z 319) of China.

References

[1] J.W. Long, B. Dunn, D.R. Rolison, H.S. White, Chem. Rev. 104 (2004) 4463–4492.
[2] M. Armand, J.M. Tarascon, Nature 451 (2008) 652–657.
[3] B.E. Conway, Electrochemical Supercapacitors: Scientific Fundamentals and Technological Applications, Kluwer, New York, 1999.
[4] P. Simon, Y. Gogotsi, Nat. Mater. 7 (2008) 845–854.
[5] M. Winter, R.J. Brodd, Chem. Rev. 104 (2004) 4245–4269.
[6] B.E. Conway, V. Birss, J. Wojtowicz, J. Power Sources 66 (1997) 1–14.
[7] E. Frackowiak, F. Beguin, Carbon 39 (2001) 937–950.
[8] D. Bélanger, T. Brousse, J.W. Long, Interface 17 (2008) 49–52.
[9] J.W. Long, D. Belanger, T. Brousse, W. Sugimoto, M.B. Sassin, O. Crosnier, MRS Bull. 36 (2011) 513–522.
[10] M.S. Hong, S.H. Lee, S.W. Kim, Electrochem. Solid State Lett. 5 (2002) A227–A230.
[11] T. Brousse, M. Toupin, D. Belanger, J. Electrochem. Soc. 151 (2004) A614–A622.
[12] V. Khomenko, E. Raymundo-Pinero, F. Beguin, J. Power Sources 153 (2006) 183–190.
[13] T. Brousse, P. Taberna, O. Crosnier, R. Dugas, P. Guillemet, Y. Scudeller, Y. Zhou, F. Favier, D. Belanger, P. Simon, J. Power Sources 173 (2007) 633–641.
[14] L. Demarconnay, E. Raymundo-Pinero, F. Beguin, J. Power Sources 196 (2011) 580–586.
[15] M. Toupin, T. Brousse, D. Belanger, Chem. Mater. 16 (2004) 3184–3190.
[16] T. Brousse, M. Toupin, R. Dugas, L. Athouel, O. Crosnier, D. Belanger, J. Electrochem. Soc. 153 (2006) A2171–A2180.
[17] H.J. In, S. Kumar, Y. Shao-Horn, G. Barbastathis, Appl. Phys. Lett. 88 (2006) 083104.
[18] Y.Q. Jiang, Q. Zhou, L. Lin, in: IEEE 22nd International Conference on Micro Electro Mechanical Systems. MEMS 2009 (2009), pp. 587–590.
[19] D. Pech, M. Brunet, P.L. Taberna, P. Simon, N. Fabre, F. Mesnilgrente, V. Conedera, H. Durou, J. Power Sources 195 (2010) 1266–1269.
[20] D. Pech, M. Brunet, H. Durou, P.H. Huang, V. Mochalin, Y. Gogotsi, P.L. Taberna, P. Simon, Nat. Nanotechnol. 5 (2010) 651–654.
[21] J. Chmiola, C. Largeot, P.L. Taberna, P. Simon, Y. Gogotsi, Science 328 (2010) 480–483.
[22] C. Shen, X. Wang, W. Zhang, F. Kang, J. Power Sources 196 (2011) 10465–10471.
[23] W. Gao, N. Singh, L. Song, Z. Liu, A.L.M. Reddy, L. Ci, R. Vajtai, Q. Zhang, B. Wei, P.M. Ajayan, Nat. Nanotechnol. 6 (2011) 496–500.
[24] W. Sun, R.L. Zheng, X.Y. Chen, J. Power Sources 195 (2010) 7120–7125.
[25] H.X. Ji, Y.F. Mei, O.G. Schmidt, Chem. Commun. 46 (2010) 3881–3883.
[26] W. Wei, X. Cui, W. Chen, D.G. Ivey, Chem. Soc. Rev. 40 (2011) 1697–1721.
[27] H.Y. Lee, J.B. Goodenough, J. Solid State Chem. 144 (1999) 220–223.